# The strain, energy band and photoluminescence of GaAs$_{0.92}$Sb$_{0.08}$/Al$_{0.3}$Ga$_{0.7}$As multiple quantum wells grown on GaAs substrate

Xian Gao [a,c], Xuan Fang [a], Jilong Tang [a], Dan Fang [a], Dengkui Wang [a], Xiaohua Wang [a], Rui Chen [c], Shijie Xu [b,**], Zhipeng Wei [a,*]

[a] State Key Laboratory of High Power Semiconductor Laser, Changchun University of Science and Technology, 7089 Wei-Xing Road, Changchun, 130022, PR China
[b] Department of Physics, University of Hong Kong, Pokfulam Road, Hong Kong, China
[c] Department of Electrical and Electronic Engineering, South University of Science and Technology of China, Shenzhen, Guangdong, 518055, PR China

## ARTICLE INFO

## ABSTRACT

GaAsSb based materials have become the promising system for infrared semiconductor lasers and detectors. In this article, the strain, energy band structures and photoluminescence (PL) of GaAs$_{0.92}$Sb$_{0.08}$/Al$_{0.3}$Ga$_{0.7}$As strained quantum wells (QWs) grown with molecular beam epitaxy are systematically analyzed both theoretically and experimentally. The theoretical results are derived by Kane's model and k·p method, and the optical properties of a high-quality GaAs$_{0.92}$Sb$_{0.08}$/Al$_{0.3}$Ga$_{0.7}$As strained QWs sample are thoroughly investigated by excitation- and temperature-dependent PL measurements. The theoretical results show the strain has significant influence on the band structure of QWs. In experimental part, it is found that the light-hole exciton emission coexists with the heavy-hole exciton line in the temperature range of 50 K–300 K. However, the emission of localized excitons, which is caused by the nonuniformity of component in the GaAsSb well layer, takes over the light-hole exciton emission at lower temperatures (<50 K).

## 1. Introduction

With the advantages of high carriers' concentration and mobility, GaAs based semiconductors have great potential in high performance optoelectronic applications [1,2]. In particular, GaAsSb alloy has drawn a great attention due to the tunable feature of band gap. Diversified quantum structures such as GaAsSb/GaAs single/multiple quantum wells (QWs) [3], W-design AlSb/InAs/GaAsSb QWs [4] and GaAsSb/InGaAs heterostructures [5] have been developed so far. Therefore, GaAsSb alloy and relevant quantum structures have been recognized as a vital material system for fabricating the infrared semiconductor lasers and detectors [6–8]. Furthermore, lattice parameter and band structure of GaAsSb based materials could be adjusted by varying antimony component. The optical properties also can be adjusted via intentional incorporation of lattice-mismatch strain in device. It is predicted that the GaAsSb-based strained QWs may take a great advantage in infrared detector and laser.

In fact, the strained quantum well structures have some great advantage for semiconductor lasers owing to the improvement in the asymmetry of conduction and valence band effective masses, inter-valence band optical absorption and Auger recombination [9–13]. Therefore, it is highly desirable to investigate the band structure and optical properties of GaAsSb-based strained quantum well structures for device applications. In literature, the optical properties of many III-V compound QWs are thoroughly investigated, including GaAs/AlGaAs, InGaAs/AlGaAs and InGaAsP [14–18]. However, the information and understanding about the band structure and optical properties of the GaAsSb-based strained QWs is still limited [19]. In particular, the investigation on the strain effect on the band structure and complicated carrier transition in GaAsSb strained QWs is also significantly insufficient.

In this article, we calculate the band structures of the GaAsSb/AlGaAs QWs with and without strain by using Kane's model and k·p method first, and then conduct an in-depth investigation on the photoluminescence (PL) properties of the GaAs$_{0.92}$Sb$_{0.08}$/Al$_{0.3}$Ga$_{0.7}$As strained MQWs grown on GaAs substrate. It is found that the strain effect shall be responsible for the valence-band splitting. The phenomenon of the valence-band splitting is verified by the PL measurements. Moreover,

---

* Corresponding author.
** Corresponding author.
   E-mail addresses: sjxu@hku.hk (S. Xu), zpweicust@126.com (Z. Wei).

the PL behaviors of heavy-hole, light-hole and localized excitons are investigated thoroughly.

## 2. The calculation of band structure

In this section, the band structure of GaAs$_{0.92}$Sb$_{0.08}$/Al$_{0.3}$Ga$_{0.7}$As QW is calculated based on k·p method with and without the strain effects. In this way, the effect of strain on the band structure can be clearly expressed. For the sake of simplicity, we constructed a model structure of GaAs$_{0.92}$Sb$_{0.08}$ layer sandwiched between two Al$_{0.3}$Ga$_{0.7}$As layers. Firstly, Kane's model is used to define the band-edge parameters in the vicinity of center of Brillouin zone. The Schrödinger equation takes the form [20]:

$$Hu_{nk}(\mathbf{r}) = \left(H_0 + \frac{\hbar^2 k^2}{2m_0} + \frac{\hbar}{m_0}\mathbf{k}\cdot\mathbf{p} + H_{SO}\right)u_{nk}(\mathbf{r}) = E_n(\mathbf{k})u_{nk}(\mathbf{r}), \tag{1}$$

where

$$H_0 = \frac{p^2}{2m_0} + V(\mathbf{r}), \tag{2}$$

and

$$H_{so} = \frac{\hbar}{4m_0^2 c^2}\Delta V \times \mathbf{p}\cdot\boldsymbol{\sigma} \tag{3}$$

Here, the second term in the middle side of equation (1) is the **k·p** interaction, the third term $H_{SO}$ represents the spin-orbit interaction, and $V(\mathbf{r})$ of equation (2) is the periodic potential. Considering the valence and conduction band interactions, the eight-by-eight interaction matrix can be written as follows:

$$\begin{bmatrix} H & H_{SO} \\ H_{SO}^* & H \end{bmatrix}, \tag{4}$$

$$H = H(k=0) + D, \tag{5}$$

where H ($k = 0$) can be expressed as

$$H(k=0) = \begin{bmatrix} E_c & iPk_x & iPk_y & iPk_z \\ -iPk_x & E_v & 0 & 0 \\ -iPk_y & 0 & E_v & 0 \\ -iPk_z & 0 & 0 & E_v \end{bmatrix} \tag{6}$$

Here *P* is the Kane's parameter. $E_c$ and $E_v$ are eigenvalues at the zone center.

$$P = \sqrt{\frac{\hbar^2}{2m_0}E_P}, \tag{7}$$

$$E_c = E_g, \quad E_v = -\Delta_{SO}/3 \tag{8}$$

The band gap of unstrained GaAs$_{1-x}$Sb$_x$ layer does not follow the Vegard's law, and may be expressed as

$$E_g = 1.43 - 1.9x + 1.2x^2 \tag{9}$$

D in equation (5) refers to the k-dependent contribution for the conduction and valence band [21]:

The fundamental band-structure parameters A$_1$, A$_2$, B$_1$, B$_2$, L$_1$, L$_2$, M$_1$, M$_2$, M$_3$, N$_1$, N$_2$, and N$_3$ are defined, which are related to the Luttinger-Kohn parameters $\gamma_1$, $\gamma_2$ and $\gamma_3$ [22].

$$A_1 = A_2 = \frac{\hbar^2}{2m_0}\left(\frac{1}{m_c} - 1\right) - \frac{P^2}{Eg}, \tag{11}$$

$$B_1 = B_2 = 0, \tag{12}$$

$$L_1 = L_2 = -\frac{\hbar^2}{2m_0}(\gamma_1 + 4\gamma_2) - \frac{P^2}{Eg}, \tag{13}$$

$$M_1 = M_2 = -\frac{\hbar^2}{2m_0}(\gamma_1 - 2\gamma_2), \tag{14}$$

$$N_1 = N_2 = -\frac{3\hbar^2}{m_0}\gamma_3 + \frac{P^2}{E_g} \tag{15}$$

$$N_3 = 0, \tag{16}$$

and $H_{SO}$ accounting for the spin-orbit interaction may be written as

$$H_{SO} = -\frac{\Delta_{SO}}{3}\begin{bmatrix} 0 & 0 & 0 & 0 \\ 0 & 0 & 0 & -1 \\ 0 & 0 & 0 & i \\ 0 & 1 & -i & 0 \end{bmatrix} \tag{17}$$

Next, the strain effects will be taken into account in this eight-by-eight Hamiltonian based on the k·p method [21]. The four-by-four Hamiltonian matrix with strain effect can be written in the following form:

$$H = H(k=0) + D + H_{strain} \tag{18}$$

Since the lattice constant *a* of GaAs$_{0.92}$Sb$_{0.08}$ is larger than Al$_{0.3}$Ga$_{0.7}$As, the strain in GaAs$_{0.92}$Sb$_{0.08}$ layer could be compressive. Considering the strain tensor, the GaAsSb layer under biaxial strain in the plane of the AlGaAs material could be described as $\varepsilon_{||}$:

$$\varepsilon_{||} = \varepsilon_{xx} = \varepsilon_{yy} = \frac{a_0 - a}{a}, \tag{19}$$

where $a_0$ and *a* are the lattice constants of the AlGaAs barrier layer and GaAsSb well layer, respectively.

The uniaxial strain in the perpendicular growth direction could be described as $\varepsilon_{\perp}$:

$$\varepsilon_{\perp} = \varepsilon_{zz} = -2\frac{C_{12}}{C_{11}}\varepsilon_{xx} \tag{20}$$

Here C$_{11}$ and C$_{12}$ are the elastic stiffness constants. All constants could be determined by the components of GaAsSb and AlGaAs, which are obtained from the lattice constant of GaAs, GaSb and AlAs according to Vegard's law.

The strain effect can be simply defined as the matrix:

$$H_{strain} = \begin{bmatrix} E_{C\_S} & 0 & 0 & 0 \\ 0 & E_{v\_S} & 0 & 0 \\ 0 & 0 & E_{v\_S} & 0 \\ 0 & 0 & 0 & \lambda\_S \end{bmatrix}, \tag{21}$$

$$D = \begin{bmatrix} A_2\left(k_x^2 + k_y^2\right) + A_1 k_z^2 & B_2 k_y k_z & B_2 k_x k_z & B_1 k_x k_y \\ B_2 k_y k_z & L_1 k_x^2 + M_1 k_y^2 + M_2 k_z^2 & N_1 k_x k_y & N_2 k_x k_z - N_3 k_x \\ B_2 k_x k_z & N_1 k_x k_y & L_1 k_y^2 + M_1 k_x^2 + M_2 k_z^2 & N_2 k_y k_z - N_3 k_y \\ B_1 k_x k_y & N_2 k_x k_z - N_3 k_x & N_2 k_y k_z - N_3 k_y & L_2 k_z^2 + M_3\left(k_x^2 + k_y^2\right) \end{bmatrix} \tag{10}$$
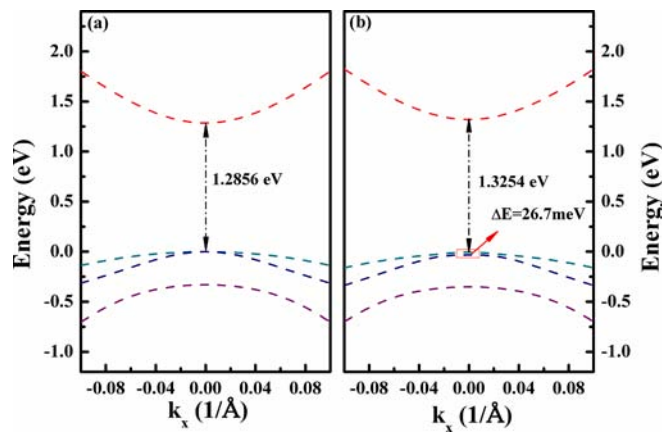
**Fig. 1.** Calculated band structures of GaAsSb/AlGaAs QW (a) without and (b) with strain.
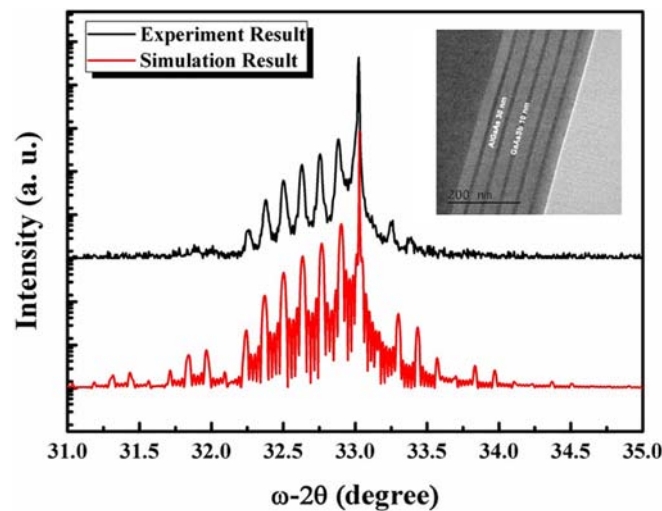


**Fig. 2.** Experimental (upper) and simulated (lower) XRD patterns of the GaAsSb/AlGaAs QWs grown with MBE. Inset sketches the TEM image of the MQWs sample.

where

$$E_{C\_}S = a_c(\varepsilon_{xx} + \varepsilon_{yy} + \varepsilon_{zz}),$$ (22)

$$E_v\_S = \lambda\_S + \theta\_S,$$ (23)

$$\lambda\_S = D_1 \varepsilon_{zz} + D_2(\varepsilon_{xx} + \varepsilon_{yy}),$$ (24)

$$\theta\_S = D_3 \varepsilon_{zz} + D_4(\varepsilon_{xx} + \varepsilon_{yy})$$ (25)

Here $D_1$, $D_2$, $D_3$ and $D_4$ are defined as the deformation potentials. The parameters used in theoretical calculations are obtained from literatures [23].

Fig. 1 shows the band-edge structure of GaAs$_{0.92}$Sb$_{0.08}$/Al$_{0.3}$Ga$_{0.7}$As QW without and with strain based on the above-described model. The band gap at the zone center of the GaAs$_{0.92}$Sb$_{0.08}$/Al$_{0.3}$Ga$_{0.7}$As QW without and with strain is computed to be 1.2856 eV and 1.3254 eV, respectively. It is clear that the valence band is spilt in the strained GaAs$_{0.92}$Sb$_{0.08}$/Al$_{0.3}$Ga$_{0.7}$As QW, and the difference of energy between heavy hole band and light hole band is 26.7 meV. Since the studied GaAsSb/AlGaAs QW has a significant amount of strain, these calculation results may be valuable to the explanation of the experimental results and functional QW device design.
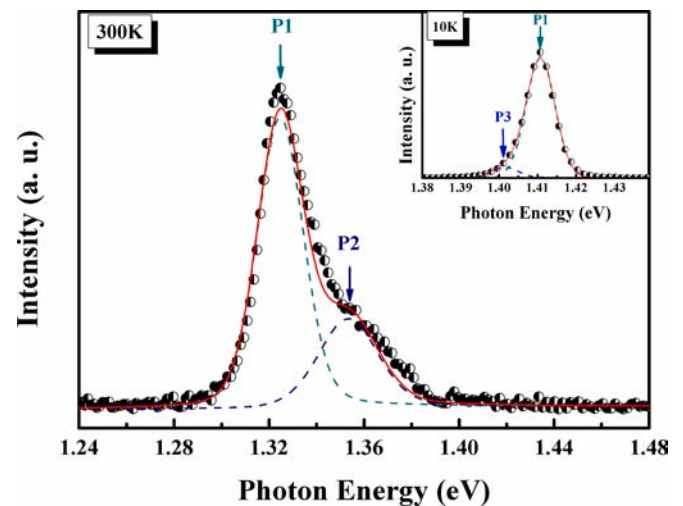


**Fig. 3.** Room temperature (300 K) PL spectrum (symbols) of the MQWs sample. The inset presents the low temperature (10 K) PL spectrum.

## 3. Experimental details

A sample of strained GaAs$_{0.92}$Sb$_{0.08}$/Al$_{0.3}$Ga$_{0.7}$As MQWs was grown on semi-insulating (001)-oriented GaAs substrate with MBE, which is composed of a 100 nm thick GaAs buffer layer and 5 periods of GaAs$_{0.92}$Sb$_{0.08}$/Al$_{0.3}$Ga$_{0.7}$As MQWs with 10 nm GaAs$_{0.92}$Sb$_{0.08}$ quantum well layer and 30 nm Al$_{0.3}$Ga$_{0.7}$As barrier layers. The thickness and crystal quality of the sample is examined by high-resolution X-ray diffraction with Cu-Ka radiation (HRXRD, Bruker D8 DAVINCI). The morphology and structure of the MQWs was measured by transmission electron microscopy (TEM, JEOL: JEM-2010F). Temperature-dependent PL measurements were performed between 10 and 300 K on a closed-cycle helium cryostat. The PL signals are dispersed by using a HORIBA iHR 550 monochromator, and detected by a Peltier cooled InGaAs detector. Standard lock-in amplifier technique was employed to enhance the signal-to-the noise ratio. The excitation source was a continuous-wave semiconductor laser diode with the emission wavelength of 655 nm, and the excitation density could be adjusted from 0.25 to 250 mW/cm$^2$.

## 4. Results and discussions

Fig. 2 shows the experiment and simulation results with $\omega$-$2\theta$ scans along GaAs (004) direction of the sample. In addition to the GaAs (004) diffraction peak from the GaAs substrate, up to six orders of satellite peaks related to the GaAs$_{0.92}$Sb$_{0.08}$/Al$_{0.3}$Ga$_{0.7}$As MQWs are clearly observed, which implies a high crystalline quality. Compared with the simulation patterns, the experimental GaAs (004) diffraction peak shows a low degree shift, indicating the existence of residual strain in the MQWs structure of sample.

The PL spectra of the sample at 300 K and 10 K are displayed in Fig. 3. It is obvious that the room-temperature spectrum is asymmetric with a high energy tail. The emission peak could be decomposed into two components P1 and P2 located at 1.325 and 1.352 eV, respectively. The origins of the two emission peaks will be discussed later. In sharp contrast to the room-temperature PL, the 10 K PL spectrum shows a low energy tail. This result suggests the different emission channels appeared at low temperature. The 10 K PL spectrum could also be decomposed into two parts, namely P1 and P3, located at 1.411 and 1.401 eV, respectively, as shown in the inset of Fig. 3.

According to the literature [24], the band alignment of GaAsSb/Al-GaAs quantum well shall be type I energy lineup. The lattice-constant mismatch between GaAsSb and AlGaAs evidenced by the HRXRD data can lead to a strain. As discussed earlier, the strain can lift up the
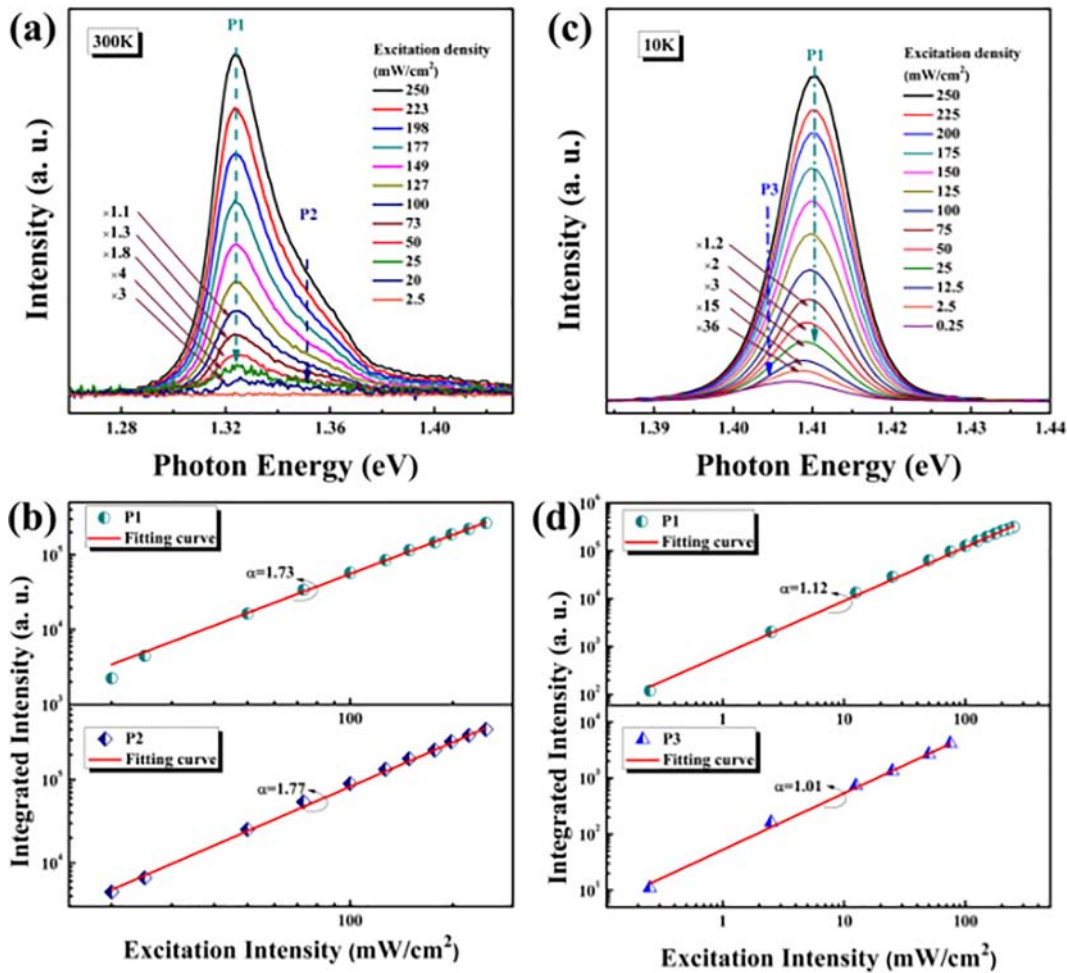
**Fig. 4.** (a) Excitation-density dependent PL spectra of the sample measured at 300 K; (b) Integrated PL intensities of P1 and P2 at 300 K; (c) Excitation-density dependent PL spectra of the sample at 10 K; (d) Integrated PL intensities of P1 and P3 at 10 K.
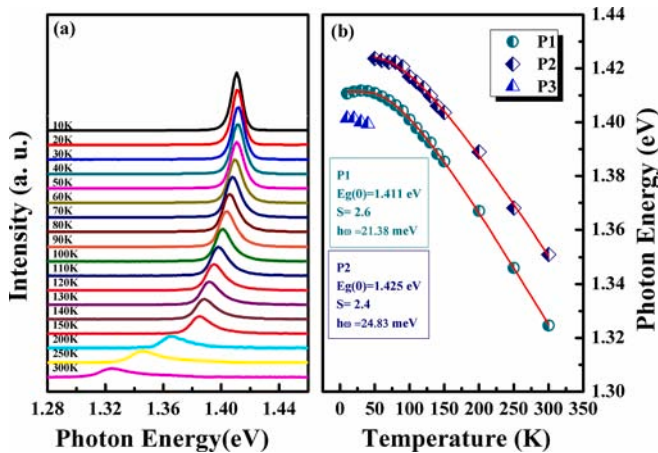


**Fig. 5.** (a) Temperature dependent PL spectra of the MQWs sample from 10 K to 300 K. (b) Temperature dependent peak position of P1, P2 and P3. Solid lines are the fitting curves.

degeneracy of valence band in GaAsSb. The band-edge energy which is obtained from the PL measurement shall thus include the strain effect. If P1 and P2 peaks in the 300 K PL spectrum are assigned to be the luminescent transitions of heavy- and light-hole subbands in $Al_{0.3}Ga_{0.7}As/GaAs_{0.92}Sb_{0.08}$ QWs sample, the energy separation between the split heavy- and light-hole subbands is about 27 meV, which is

in good agreement with the theoretical value (e.g. 26.7 meV). Such good agreement between experiment and theory, in turn, makes us confident for the assignments of P1 and P2 luminescence peaks. As discussed below, excitation-dependent PL spectra are analyzed for further investigation of the origins of these peaks.

Fig. 4(a) displays the excitation-dependent PL spectra of the sample measured at 300 K, in which the peaks of P1 and P2 are seen clearly. The PL intensities of peak P1 and P2 versus the excitation density are depicted in Fig. 4(b). The trend of integrated PL intensity $I$ of emission with the excitation density $I_0$ could be represented by Ref. [25].

$$I = \eta I_0^\alpha \tag{26}$$

Value of the power index $\alpha$ may indicate the radiative recombination mechanism. For the excitonic recombination, $1 < \alpha < 2$, while for the direct band gap emission, $\alpha \approx 2$ [26]. The solid lines in Fig. 4(b) stand for the best fitting curves with equation (26) and the values of parameter $\alpha$ are 1.73 and 1.77 for P1 and P2. Obviously, these values support the assignment of excitonic recombination. Fig. 4(c) shows the excitation-dependent PL spectra of the sample at 10 K. It is worth to note that an excitation-dependent blueshift is observed. Considering the type I band alignment of GaAsSb/AlGaAs quantum well, we attributed this blueshift to the band-filling effect of localized states in the GaAsSb well layer [27–29]. In Fig. 4(d), the integrated PL intensities of P1 and P3 are plotted, and the values of parameter $\alpha$ are determined to be 1.12 and 1.01 for P1 and P3, respectively. The obtained $\alpha$ value also suggests that P1 and P3 peaks shall be ascribed to the excitonic recombination. In order to further look at the origins of P1, P2 and P3,

temperature-dependent PL spectra are investigated.

Fig. 5(a) presents temperature-dependent PL spectra of the sample. It is interesting to note that the spectra display a low energy tail in the low temperature range of 10–40 K. However, the low energy tail disappeared when the temperatures higher than 50 K. The transition of asymmetrical PL line shape also suggests that the emission should have different recombination mechanisms. For example, P3 is thermally quenched at 50 K, while P2 becomes observable. Note that P1 always keeps its dominant role in the PL spectra in the interested temperature range. To understand the evolution mechanisms of these PL peaks, temperature dependent peak energies are examined below.

The peak emission energies of P1, P2 and P3 obtained from Fig. 5(a) are plotted in Fig. 5(b). The solid lines represent the theoretical curves with the equation [30].

$$E_g(T) = E_g(0) - S < h\omega > \left( \coth \frac{< h\omega >}{2kT} - 1 \right), \tag{27}$$

where $E_g(0)$ is the band gap of the sample at 0 K, $S$ describes the dimensionless electron-phonon coupling constant, and $< h\omega >$ represents an average phonon energy involved within radiative recombination process. The values of $< h\omega >$ are obtained to be 21.38 meV and 24.83 meV for P1 and P2, respectively. The values of $Eg(0)$ calculated to be 1.425 meV for P2, is larger than the bandgap of $GaAs_{0.92}Sb_{0.08}$, which is attribute to the quantum confinement. It is noted that reasonably good agreement between experiment and model is achieved, indicating that temperature dependence of P1 and P2 peak position complies with that of the band gap. As for the existence of localized excitons in the low temperature range, it can be well understood in terms of the non-uniformity of components in GaAsSb layer [27].

## 5. Conclusion

In conclusion, the strain effect in $GaAs_{0.92}Sb_{0.08}/Al_{0.3}Ga_{0.7}As$ MQWs sample is analyzed by band structure calculation, XRD and PL measurement. The experimental XRD data and simulation results show clear evidence of the existence of compressive strain in the MQWs sample. At room temperature, the energy deviation between the heavy-hole and light-hole emission peaks in the measured PL spectrum is in good agreement with the calculation result when a strain is taken into account. Excitation- and temperature-dependent PL spectra give important information on the nature of emission peaks in the studied $GaAs_{0.92}Sb_{0.08}/Al_{0.3}Ga_{0.7}As$ strained MQWs sample. The results and new understanding presented in this study could be helpful for the design and fabrication of GaAsSb based optoelectronic and photonic devices.

## Declaration of competing interest

The authors declare that there are no conflicts of interest.

## References

[1] J. Yoon, S. Jo, I.S. Chun, I. Jung, H.S. Kim, M. Meitl, E. Menard, X. Li, J.J. Coleman, U. Paik, J.A. Rogers, Nature 465 (2010) 329–333.
[2] A.J. Ritenour, S. Levinrad, C. Bradley, R.C. Cramer, S.W. Boettcher, ACS Nano 7 (2013) 6840–6849.
[3] A.R. Kost, X. Sun, N. Peyghambarian, N. Eradat, E. Selvig, B.O. Fimland, D.H. Chow, Appl. Phys. Lett. 85 (2004) 5631–5633.
[4] M. Motyka, M. Dyksik, K. Ryczko, R. Weih, M. Dallner, S. Höfling, M. Kamp, G. Sęk, J. Misiewicz, Appl. Phys. Lett. 108 (2016), 101905.
[5] C. Deutsch, A. Benz, H. Detz, P. Klang, M. Nobile, A.M. Andrews, W. Schrenk, T. Kubis, P. Vogl, G. Strasser, K. Unterrainer, Appl. Phys. Lett. 97 (2010), 261110.
[6] J. Huh, H. Yun, D.C. Kim, A.M. Munshi, D.L. Dheeraj, H. Kauko, A.T.J. van Helvoort, S. Lee, B.O. Fimland, H. Weman, Nano Lett. 15 (2015) 3709–3715.
[7] V. Fathipour, S.J. Jang, I.H. Nia, H. Mohseni, Appl. Phys. Lett. 106 (2015), 021116.
[8] M.K. Hudait, Y. Zhu, P. Goley, M. Clavel, N. Jain, APEX 8 (2015), 025501.
[9] Y. Arakawa, H. Sakaki, Appl. Phys. Lett. 40 (1982) 939–941.
[10] E. Yablonovitch, E.O. Kane, J. Light. Technol. 6 (1988) 1292–1299.
[11] R. Moriya, K. Sawano, Y. Hoshi, S. Masubuchi, Y. Shiraki, A. Wild, C. Neumann, G. Abstreiter, D. Bougeard, T. Koga, et al., Phys. Rev. Lett. 113 (2014), 086601.
[12] B.A. Bernevig, T.L. Hughes, S.C. Zhang, Science 314 (2006) 1757–1761.
[13] L. Colombo, R. Resta, S. Baroni, Phys. Rev. B 44 (11) (1991) 5572.
[14] J.W. Luo, G. Bester, A. Zunger, Phys. Rev. B 92 (2015), 165301.
[15] R. Fiederling, M. Keim, G. Reuscher, W. Ossau, G. Schmidt, A. Waag, L.W. Molenkamp, Nature 402 (1999) 787–790.
[16] A.H. Quarterman, K.G. Wilcox, V. Apostolopoulos, Z. Mihoubi, S.P. Elsmere, I. Farrer, D.A. Ritchie, A. Tropper, Nat. Photonics 3 (2009) 729–731.
[17] T. Ishikawa, J.E. Bowers, IEEE J. Quantum Electron. 30 (1994) 562–570.
[18] S. Ke, R. Wang, M. Huang, Phys. Rev. B 49 (1994) 10495.
[19] T.S. Wang, J.T. Tsai, K.I. Lin, J.S. Hwang, H.H. Lin, L.C. Chou, Mater. Sci. Eng. B 147 (2008) 131–135.
[20] E.O. Kane, J. Phys. Chem. Solids 1 (1957) 249–261.
[21] S.L. Chuang, C.S. Chang, Phys. Rev. B 54 (1996) 2491–2504.
[22] J.M. Luttinger, W. Kohn, Phys. Rev. 97 (1955) 869–883.
[23] I. Vurgaftman, J.R. Meyer, L.R. Ram-Mohan, J. Appl. Phys. 89 (2001) 5815–5875.
[24] R. Teissier, D. Sicault, J.C. Harmand, G. Ungaro, G.L. Roux, L. Largeau, J. Appl. Phys. 89 (2001) 5473–5477.
[25] T. Schmidt, K. Lischka, W. Zulehner, Phys. Rev. B 45 (1992) 8989–8994.
[26] L. Bergman, X.B. Chen, J.L. Morrison, J. Huso, A.P. Purdy, J. Appl. Phys. 96 (2004) 675–682.
[27] X. Gao, Z.P. Wei, F.H. Zhao, Y.H. Yang, R. Chen, X. Fang, J.L. Tang, D. Fang, D.K. Wang, R.X. Li, X.T. Ge, X.H. Ma, X.H. Wang, Sci. Rep. 6 (2016) 29112.
[28] Z.C. Su, J.Q. Ning, Z. Deng, X.H. Wang, S.J. Xu, R.X. Wang, S.L. Lu, J.R. Dong, H. Yang, Nanoscale 8 (2016) 7113–7118.
[29] Q. Li, S.J. Xu, M.H. Xie, Y. Tong, J. Phys. Condens. Matter 17 (2005) 4853.
[30] K.P. O'Donnell, X. Chen, Appl. Phys. Lett. 58 (1991) 2924–2926.